LETTERS

Metabolic gene regulation in a dynamically changing environment

Matthew R. Bennett[1,2]*, Wyming Lee Pang[1]*†, Natalie A. Ostroff[1], Bridget L. Baumgartner[1], Sujata Nayak[1], Lev S. Tsimring[2] & Jeff Hasty[1,2]

Natural selection dictates that cells constantly adapt to dynamically changing environments in a context-dependent manner. Gene-regulatory networks often mediate the cellular response to perturbation[1–3], and an understanding of cellular adaptation will require experimental approaches aimed at subjecting cells to a dynamic environment that mimics their natural habitat[4–9]. Here we monitor the response of *Saccharomyces cerevisiae* metabolic gene regulation to periodic changes in the external carbon source by using a microfluidic platform that allows precise, dynamic control over environmental conditions. We show that the metabolic system acts as a low-pass filter that reliably responds to a slowly changing environment, while effectively ignoring fast fluctuations. The sensitive low-frequency response was significantly faster than in predictions arising from our computational modelling, and this discrepancy was resolved by the discovery that two key galactose transcripts possess half-lives that depend on the carbon source. Finally, to explore how induction characteristics affect frequency response, we compare two *S. cerevisiae* strains and show that they have the same frequency response despite having markedly different induction properties. This suggests that although certain characteristics of the complex networks may differ when probed in a static environment, the system has been optimized for a robust response to a dynamically changing environment.

To probe the response of a metabolic gene network to a fluctuating environment, we developed a microfluidic platform that can subject a population of cells to a continuously varying supply of medium (Fig. 1). The device is designed to generate a fluctuating signal of medium by dynamically combining two medium-filled reservoirs in accordance with a time-dependent function. Feeding channels deliver the media downstream to a customizable growth chamber, which for this study was constructed to constrain a population of yeast cells to grow in a monolayer, permitting long-term data acquisition[10]. The composition of the medium is dynamically controlled by a fluidic switch[11], such that changes in the upstream source may be detected almost immediately by the cells. The fluidic switch was optimized to generate a linear range of mixing ratios from the two media inputs, allowing a variety of periodic waveforms or random signals to be generated (see Supplementary Information for full details of the device).

As a quantifiable reporter of the cellular response to environmental fluctuations, we fused the native Gal1 protein of *S. cerevisiae* to the yeast-optimized enhanced cyan fluorescent protein (yECFP)[12,13]. The enzymes for galactose utilization, including Gal1, are among the most tightly regulated proteins in yeast. Because glucose requires much less energy to metabolize, cells will consume galactose only if glucose is not available. *S. cerevisiae* has therefore evolved a highly complex regulatory network to ensure that the galactose-metabolizing enzymes will be strongly activated when they are needed, but tightly repressed if glucose is present in the environment (Fig. 2a). Because the network has been well studied and involves regulatory motifs common to many higher organisms, galactose utilization is a model for gene regulation. To build on the current understanding of its robust regulatory mechanisms, we employed our microfluidic platform to monitor the dynamics of network activation and repression in response to sinusoidal perturbations of glucose over a galactose background.

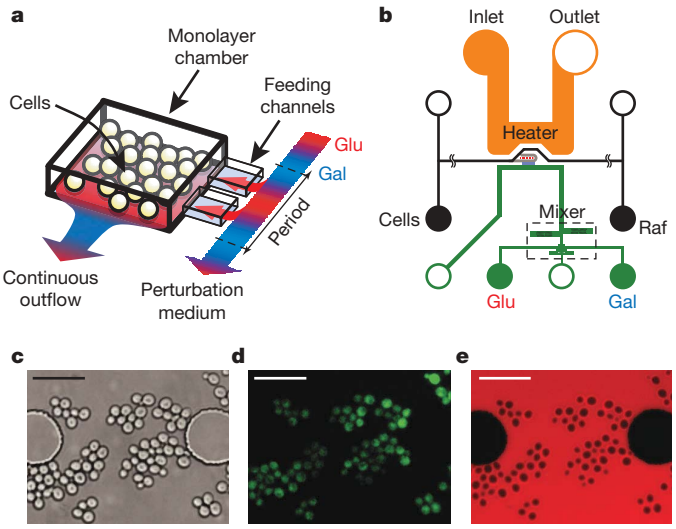

Figure 1 | Design and implementation of the microfluidic platform developed for our study. a, Conceptual design of the imaging chamber. The chamber is coupled to the switch output channel by means of multiple 'feeding' channels 1 μm tall. The feeding channels are fed by a controllable waveform generator that creates sinusoidal perturbations in the glucose concentration while maintaining constant background levels of galactose. **b**, An overview of the design showing the layout of the device. The device makes use of three flow networks for loading cells (middle, black), generating microenvironmental waveforms (bottom, green), and controlling on-chip temperature (top, orange). The imaging chamber (centre, grey region) is designed to be about 4 μm tall to constrain a population of yeast cells to grow in a monolayer. **c**, Representative bright-field image of cells growing in the imaging chamber. These images were used to measure the total size of the colony. Large circles are support posts in the chamber. Scale bar, 25 μm. **d**, Green fluorescence image of the same cells as in **c**. These images allowed us to measure the amount of Gal1 in each cell. **e**, Red fluorescence image of the chamber. The glucose medium also contained a red fluorescent dye; the intensity of the red fluorescence was therefore proportional to the amount of glucose in the chamber at any given time.

[1]Department of Bioengineering, and [2]Institute for Nonlinear Science, University of California, San Diego, La Jolla, California 92093, USA. †Present address: Institute for Systems Biology, Seattle, Washington 98103, USA.
* These authors contributed equally to this work.

A population of yeast cells was subjected to sinusoidal waves of glucose concentration over a 0.2% (w/v) galactose background, with glucose concentration varying from 0% (no repression of *GAL1* transcription) to 0.25% (full repression; see Supplementary Information for repression data). For each run we changed the frequency of the glucose signal, varying the period from 0.75 to 4.5 h, and we imaged the population for a minimum of four full cycles. Time-lapse fluorescence imaging of the cell population in the growth chamber was used to calculate the amplitude ratio and phase shift of the cellular response relative to the glucose signal. The results show a maximum response frequency of about 5.6 radians h^{-1} (1.125 h period). At this frequency, the response trace was indistinguishable from a normal step-function response, whereas at the lower frequencies the temporal fluorescence trajectories clearly oscillated in response to the signal. In this sense, the galactose system seems to function as a low-pass filter that reliably responds to a slowly changing environment, while effectively ignoring fluctuations that are too fast for the cell to mount an efficient response.

Because the sinusoidal driving of the galactose utilization network leads to complex cellular behaviour, we used computational modelling to simulate the response and to uncover key aspects of the network architecture that give rise to the observed behaviour[14]. In particular, we were interested in how the interplay of the galactose and glucose utilization networks gives rise to the observed frequency response to carbon source fluctuations. By itself, the turnover of Gal1–yECFP, due either to dilution or to active degradation (or both), leads to low-pass filtering of periodic signals. However, feedback loops inherent in gene regulatory networks can alter the response of proteins to stimuli[15]. Therefore, to simulate the effects of galactose activation and glucose repression on our experimental data, we adapted a comprehensive model of the galactose network described previously[16]. This model includes the transcription and translation of the *GAL1*, *GAL2*, *GAL3*, *GAL4* and *GAL80* genes as well as the interactions of their respective proteins with each other and with galactose (such as dimerization, transport and metabolism). Whenever possible we used parameter values either at or close to the values reported previously[16]. In addition to this galactose network model, it was necessary to model the dynamics of the glucose network. The glucose network is much more complex than that of galactose[17–19] and models for it are much less well established. We therefore chose to model the glucose network with a simplified module describing a basic transport regulatory system. In it, protein products of the glucose network are responsible for transporting external glucose into the cell while internalized glucose acts to induce transcription in the network, giving rise to a positive feedback loop (see Fig. 2a).

Calibration of the computational model to the experimental data led to several important observations that would not have arisen from an analysis of steady-state batch culture data. The large amplitude ratios observed at low frequencies suggested that when glucose was added to the system the degradation rates of some galactose network components were greater than in the absence of glucose. Previous studies have suggested that components of the glucose network can actively degrade messenger RNA produced by genes involved in the galactose/glucose switch[8], and this phenomenon has also been shown to exist for the mRNA of other genes[20–22]. We therefore added enzymatic decay terms (governed by Michaelis–Menten dynamics) to the equations describing the dynamics of the *GAL1* and *GAL3* mRNA and found that it greatly increased the accuracy of the model. These two genes are among those in the galactose network that are targeted by the glucose-induced protein Mig1, which represses transcription by binding to upstream regulatory sites[19]. Thus, if proteins from the glucose network do actively degrade galactose network transcripts, *GAL1* and *GAL3* are likely targets. To test this prediction, we measured the degradation rates of *GAL1* and *GAL3* in both galactose and glucose. Both transcripts showed a 2–8-fold increase in their decay rates in the presence of glucose (see Fig. 2b and Supplementary Information), which is consistent with the values predicted by the computational model. This form of post-transcriptional regulation, in which glucose acts to downregulate Gal protein synthesis, is a previously unknown source of regulation in the galactose utilization network. Furthermore, the inclusion of glucose-mediated mRNA decay results in a model that accurately reproduces the dynamic response of a population of cells to sinusoidal repression over a large range of frequencies (Fig. 3).

Batch-culture induction characteristics for metabolic genes can vary from strain to strain or depend sensitively on the growth state of the culture. We were therefore also interested in using the model to determine how galactose induction differences would affect the response to the glucose fluctuations. The model demonstrated that

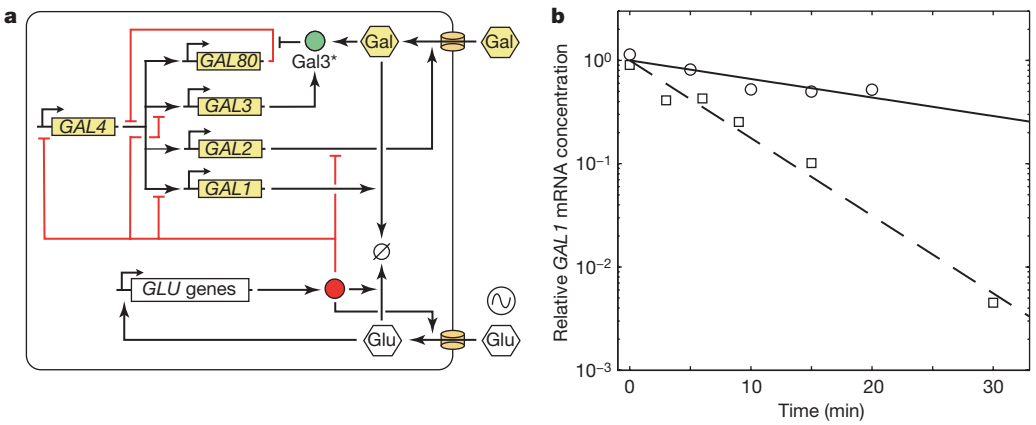

Figure 2 | Regulation in the galactose utilization network. a, Diagram of the gene regulatory networks involved. The regulatory genes in the galactose network are activated by the Gal4 protein, which binds to upstream activation sites. The *GAL80* gene provides negative feedback in the system by prohibiting the inducing affects of Gal4. Positive feedback is provided by both *GAL2* and *GAL3*. Internalized galactose can bind to Gal3, and the resulting complex binds to Gal80. Gal80 bound to the Gal3–galactose complex is incapable of repressing Gal4. In addition, the transporter Gal2 increases the amount of internal galactose, which stimulates the galactose network. The glucose network inhibits the transport of galactose and represses transcription of the galactose network in the presence of glucose through the action of Mig1, which can bind to upstream regulatory sites of *GAL1*, *GAL3* and *GAL4* (ref. 19). The glucose network also regulates the hexose transporter genes (*HXT*), responsible for transporting glucose into the cell[27], which then activates the glucose network. **b**, Experimentally measured decay of *GAL1* transcripts in galactose (circles) and glucose (squares). Also shown are the best-fit lines corresponding to half-lives of about 17 min in galactose (solid line) and 4 min in glucose (dashed line), which are similar to the values predicted by the numerical model. Data are normalized to the initial concentration of mRNA predicted by the best-fit lines. Similar results for *GAL3* transcripts are shown in Supplementary Information.

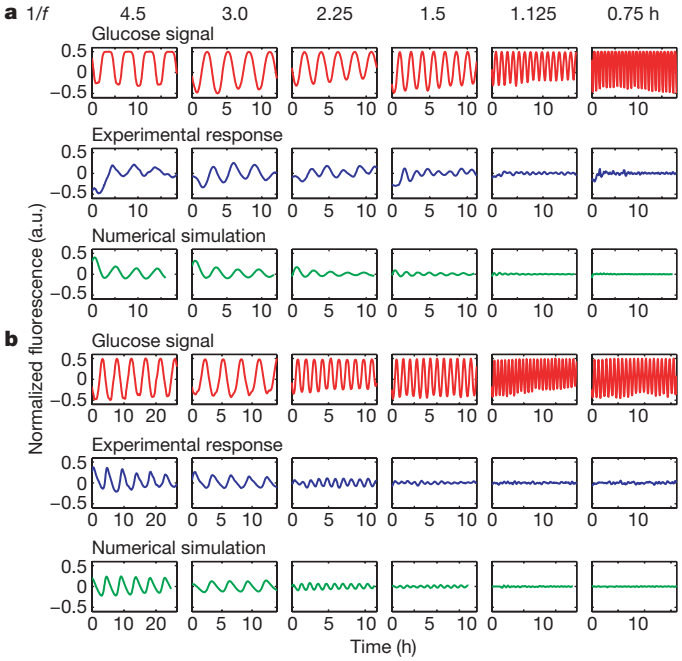

Figure 3 | Experimental and computational results for cells of two yeast strains expressing a *GAL1–yECFP* fusion gene in response to alternating glucose and galactose media. **a**, Strain K699; **b**, strain YPH499. The top row for each strain depicts the input glucose signal that was measured during each experimental run and was also used to simulate the responses. The mean fluorescence of a red tracer dye, representing the glucose concentration in the medium, is normalized and subtracted from 1 to represent the 'induction' signal used in the experimental and computational runs above. The middle rows show normalized and detrended fluorescence trajectories for a population of cells as they respond to glucose waves of various frequencies over a galactose background. In the absence of glucose, galactose induces the transcription of *GAL1–yECFP*, causing an increase in cellular fluorescence. However, as glucose is introduced into the extracellular environment, transcription of the galactose enzymes is shut off, causing a decrease in fluorescence signal as the Gal1–yECFP protein is degraded. Oscillation periods are (from left to right) 4.5, 3.0, 2.25, 1.5, 1.125 and 0.75 h. For input waves with a period shorter than 1.125 h, cells no longer responded to sinusoidal repression in a periodic fashion, demonstrating their ability to 'filter' out high-frequency environmental fluctuations. The bottom rows show simulation results for the same frequencies as above. The model, calibrated to experimental induction and repression data, accurately reproduces the cellular responses over a large range of frequencies.

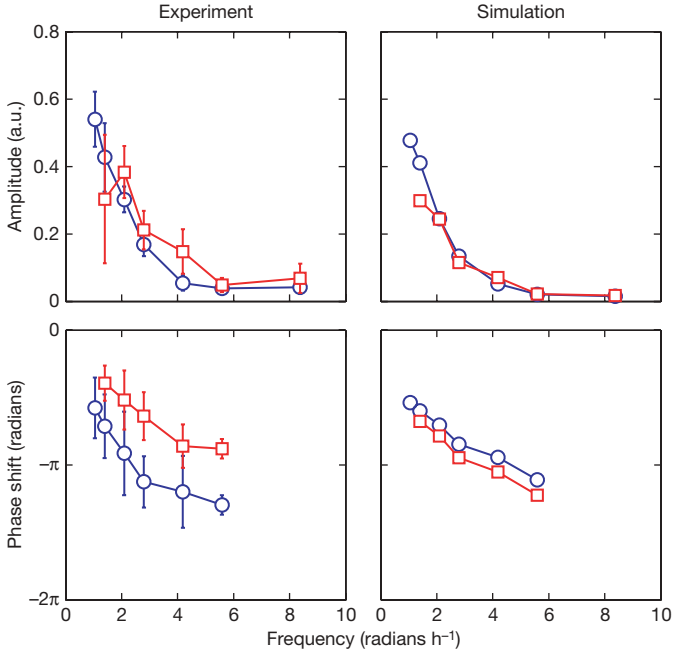

Figure 4 | Experimental and computational comparison of two yeast strains. The amplitude (top row) and phase shift (bottom row) of the response of cells to sinusoidal repression at various frequencies are shown for both K699 (red) and YPH499 (blue) strains (error bars represent s.d.). Strain YPH499 is known to have a deficiency in the galactose utilization network. For the highest-frequency trial, reliable phases could not be calculated because of noise; these results have been omitted from the graphs. The experimental data (left column) show that the amplitude responses of the two strains are strikingly similar, especially considering their significantly different induction curves (see Supplementary Information). This phenomenon was predicted by model simulations, because slight modifications to the model parameters that affected the induction and repression curves did not affect the cell population's robust response to a dynamic environment. This suggests that the complex structure of the glucose and galactose networks may confer robustness on cells even if faced with seemingly detrimental network deficiencies. The phase responses (bottom row) of the two strains showed a marked difference, with YPH499 cells having a greater phase lag than K699 cells.

significantly different galactose induction does not necessarily lead to significant differences in the response characteristics (data not shown). In other words, the model led to the hypothesis that deficiencies in network induction capabilities might not hinder a cell's ability to adapt and thrive in a changing environment. The yeast strain used to collect the present data, K699, is sensitive to external galactose concentrations, with full induction of the galactose network occurring at about 0.05% (w/v) galactose. To test our hypothesis, we turned to a strain (YPH499) that is known to have a deficiency in the galactose utilization network that causes it to require more galactose than 'normal' to induce production of the galactose enzymes[23]. YPH499 is a derivative of a *GAL2* mutant strain, and although the mutations were reportedly repaired, the *GAL2* alleles in many of the derivative strains have been shown to cause significantly impaired galactose uptake[23]. Gal2 protein is responsible for the transport of extracellular galactose into the cell and its activity is markedly different in YPH499 from that in K699. Our flow cytometry population data demonstrated that YPH499 cells require about tenfold more galactose than K699 cells to reach full induction (see Supplementary Information).

Despite the difference in induction sensitivity between K699 and YPH499 cells, our model predicted that inefficient Gal2 transport does not translate into a less robust response to a fluctuating environment. This suggests that the complex interplay of the glucose and galactose networks may confer robustness on cells even if faced with deficiencies in the induction characteristics. To validate this finding, we repeated the microfluidic runs at each frequency, this time using the YPH499 strain with a Gal1–yECFP fusion. As predicted, the amplitude responses of the two strains are strikingly similar (Fig. 4), especially considering the significant difference in their galactose sensitivity. We do not at present know the underlying mechanistic property of the regulatory network that leads to the robust response of the two strains. Future studies might endeavour to deduce this mechanism through the systematic deconstruction of the regulatory elements in a single strain. Although the present study shows how robustness can occur despite large differences in induction characteristics, one could further investigate the generality of this phenomenon by comparing the responses of many different strains to different types of temporal perturbation.

METHODS SUMMARY

Dynamic environment experiments. Cells containing a *GAL1–yECFP* fusion were imaged every 5 min for up to 24 h by using time-lapse fluorescent microscopy to estimate the concentration of Gal1 as a function of time. Cells were constrained to grow in a custom-designed microfluidic platform that permitted the dynamically controlled mixing of two growth media. Our inducing medium contained

2% raffinose and 0.2% galactose, whereas the repressing medium contained 2% raffinose, 0.2% galactose and 0.25% glucose. The resulting images were processed with cell segmentation and tracking software, and the population-averaged fluorescence concentrations were measured. To ensure correct waveform generation, glucose concentrations were monitored by introducing a red fluorescent tracer dye (sulphorhodamine 101, 0.01 mg ml^{-1}) to the repressing medium.

Microfluidic chips and waveform generation. The polydimethylsiloxane microfluidic devices were designed to permit the monolayer growth of yeast cells in the imaging chamber and were fabricated with standard replica-moulding techniques[24–26]. An upstream fluidic switch controlled the input of medium into the chamber by mixing the flows of the inducing and repressing media. The mixing ratio of the two media was governed by a software-controlled, custom-designed pressurization system that was able to produce time-varying waveforms consistently.

mRNA degradation experiments. The degradation rates of *GAL1* and *GAL3* transcripts were measured with standard reverse-transcriptase-mediated quantitative polymerase chain reaction techniques. Knockout strains for both genes were first created, and then ectopic *GAL1* and *GAL3* were placed back into the cell under the control of a doxycycline-repressible promoter. Half-lives of mRNAs were measured from cells grown in the presence or absence of glucose.

Complete details of all materials and methods used and the specifics of the computational model are available in Supplementary Information.

Received 14 April; accepted 25 June 2008.
Published online 30 July 2008.

1. Beadle, G. W. & Tatum, E. L. Genetic control of biochemical reactions in *Neurospora. Proc. Natl Acad. Sci. USA* **27,** 499–506 (1941).
2. Jacob, F. & Monod, J. Genetic regulatory mechanisms in the synthesis of proteins. *J. Mol. Biol.* **3,** 318–356 (1961).
3. Douglas, H. C. & Hawthorne, D. C. Regulation of genes controlling synthesis of the galactose pathway enzymes in yeast. *Genetics* **54,** 911–916 (1966).
4. Thattai, M. & Shraiman, B. I. Metabolic switching in the sugar phosphotransferase system of *Escherichia coli. Biophys. J.* **85,** 744–754 (2003).
5. Lipan, O. & Wong, W. H. The use of oscillatory signals in the study of genetic networks. *Proc. Natl Acad. Sci. USA* **102,** 7063–7068 (2005).
6. Kussell, E. & Leibler, S. Phenotypic diversity, population growth, and information in fluctuating environments. *Science* **309,** 2075–2078 (2005).
7. Kruse, K. & Julicher, F. Oscillations in cell biology. *Curr. Opin. Cell Biol.* **17,** 20–26 (2005).
8. Ronen, M. & Botstein, D. Transcriptional response of steady-state yeast cultures to transient perturbations in carbon source. *Proc. Natl Acad. Sci. USA* **103,** 389–394 (2006).
9. Thattai, M. & van Oudenaarden, A. Stochastic gene expression in fluctuating environments. *Genetics* **167,** 523–530 (2004).
10. Cookson, S., Ostroff, N., Pang, W. L., Volfson, D. & Hasty, J. Monitoring dynamics of single-cell gene expression over multiple cell cycles. *Mol. Syst. Biol.* **1,** doi:10.1038/msb4100032 (2005).
11. Groisman, A. *et al.* A microfluidic chemostat for experiments with bacterial and yeast cells. *Nature Methods* **2,** 685–689 (2005).
12. Sheff, M. A. & Thorn, K. S. Optimized cassettes for fluorescent protein tagging in *Saccharomyces cerevisiae. Yeast* **21,** 661–670 (2004).
13. Raser, J. M. & O'Shea, E. K. Control of stochasticity in eukaryotic gene expression. *Science* **304,** 1811–1814 (2004).
14. Hasty, J., McMillen, D., Isaacs, F. & Collins, J. J. Computational studies of gene regulatory networks: *in numero* molecular biology. *Nature Rev. Genet.* **2,** 268–279 (2001).
15. Savageau, M. A. Comparison of classical and autogenous systems of regulation in inducible operons. *Nature* **252,** 546–549 (1974).
16. de Atauri, P., Orrell, D., Ramsey, S. & Bolouri, H. Evolution of 'design' principles in biochemical networks. *Syst. Biol.* **1,** 28–40 (2004).
17. Demir, O. & Kurnaz, I. A. An integrated model of glucose and galactose metabolism regulated by the *GAL* genetic switch. *Comput. Biol. Chem.* **30,** 179–192 (2006).
18. Kaniak, A., Xue, Z., Macool, D., Kim, J. & Johnston, M. Regulatory network connecting two glucose signal transduction pathways in *Saccharomyces cerevisiae. Eukaryot. Cell* **3,** 221–231 (2004).
19. Verma, M., Bhat, O. J. & Venkatesh, K. V. Steady-state analysis of glucose repression reveals hierarchical expression of proteins under Mig1p control in *Saccharomyces cerevisiae. Biochem. J.* **388,** 843–849 (2005).
20. Scheffler, I. E., de la Cruz, B. J. & Preito, S. Control of mRNA turnover as a mechanism of glucose repression in *Saccharomyces cerevisiae. Biochem. Cell Biol.* **30,** 1175–1193 (1998).
21. de la Cruz, B. J., Prieto, S. & Scheffler, I. E. The role of the 5′ untranslated region (UTR) in glucose-dependent mRNA decay. *Yeast* **19,** 887–902 (2002).
22. Andrade, R. P., Kötter, P., Entian, K. D. & Casal, M. Multiple transcripts regulate glucose-triggered mRNA decay of the lactate transporter *JEN1* from *Saccharomyces cerevisiae. Biochem. Biophys. Res. Commun.* **332,** 254–262 (2005).
23. Rohde, J. R., Trinh, J. & Sadowski, I. Multiple signals regulate *GAL* transcription in yeast. *Mol. Cell. Biol.* **20,** 38803886 (2000).
24. Whitesides, G. M., Ostuni, E., Takayama, S., Jiang, X. Y. & Ingber, D. E. Soft lithography in biology and biochemistry. *Annu. Rev. Biomed. Eng.* **3,** 335–373 (2001).
25. Whitesides, G. M. *et al.* Soft lithography and bioanalysis. *Abstr. Pap. Am. Chem. Soc.* **227,** U113–U113 (2004).
26. Xia, Y. & Whitesides, G. M. Soft lithography. *Angew. Chem. Int. Edn Engl.* **37,** 550–575 (1998).
27. Boles, E. & Hollenberg, C. P. The molecular genetics of hexose transport in yeasts. *FEMS Microbiol. Rev.* **21,** 85–111 (1997).

Supplementary Information is linked to the online version of the paper at www.nature.com/nature.

Acknowledgements We thank A. Groisman for useful discussions regarding microfluidic design; D. Volfson and C. Grilly for aid in development and testing of image segmentation and tracking algorithms, and M. Ferry for his suggestions on microbiology. This work was supported by the National Institute of General Medical Sciences of the National Institutes of Health.

Author Information Reprints and permissions information is available at www.nature.com/reprints. Correspondence and requests for materials should be addressed to J.H. (hasty@ucsd.edu).

Metabolic gene regulation in a dynamically changing environment (supplementary information)

Matthew R. Bennett[1,2,*], Wyming Lee Pang[1,3,*], Natalie A. Ostroff[1], Bridget L. Baumgartner[1], Sujata Nayak[1], Lev S. Tsimring[2] & Jeff Hasty[1,2]

1. Department of Bioengineering, University of California, San Diego, La Jolla, CA 92093
2. Institute for Nonlinear Science, University of California, San Diego, La Jolla, CA 92093
3. Current address: Institute for Systems Biology, Seattle, WA, 98103

* These authors contributed equally to this work.

Cell preparation and experimental conditions

Transforming DNA to create fluorescent protein (FP) fusion proteins was prepared by PCR amplification of linker + FP sequence + marker sequence found on the pKT0101 plasmid[1]. PCR primers were designed with approximately 40 bp of sequence homologous to the carboxy-terminus of the target gene. Cells were transformed with the PCR product using the Lithium Acetate method, and the FP and marker sequence integrated into the genome downstream of the gene of interest by homologous recombination. Transformants were selected for histidine auxotrophy and screened for proper fluorescence under inducing conditions.

Successful transformants were grown on synthetic dropout plates at 30°C for 1–2 days and stored at 4°C for no longer than two weeks. One day prior to each experiment, an isolated colony was inoculated into liquid medium containing 2% (w/v) raffinose at 30°C at 300 rpm overnight. On the experiment day, the overnight culture was diluted to an OD_{600} 0.1 (if necessary) and grown to OD_{600} 0.3–0.6 to ensure log phase growth. Prior to loading cells onto the microfluidic device, the cell suspension was synchronized by spiking the culture with 10 nM α_1-mating factor and incubated for an additional hour.

Each experiment utilized three growth conditions: loading media, 2% raffinose; inducing media, 2% raffinose + 0.2% galactose; and repressing media, 2% raffinose + 0.2% galactose + 0.25% glucose. All media conditions were synthetic dropout based with appropriate supplements for auxotrophic selection. To maintain growth arrest during microfluidic device initialization, the loading media was also spiked with 10nM α_1-mating factor.

Data acquisition and analysis

Tracking of on-chip glucose concentration was done using a red fluorescent tracer dye (0.01 mg/mL, sulforhodamine 101) in the repressing media. Because of the similarity between the molecular weights of the dye (∼600 Da) and glucose (∼200 Da), as well as their hydrophilicity, it was assumed that the molecular diffusion/dispersion rates and aqueous partitioning coefficients of both species were identical. Prior to using sulforhodamine, Rhodamine-B was used[2]. However, this dye was

found to be slightly hydrophobic, causing it to adsorb into the PDMS, resulting in a significant amount of residual fluorescence despite several washings with undyed media. The other commonly used tracing dye, fluorescein[3, 4, 5], could not be used since it's excitation and emission spectra overlapped with the fluorescent protein reporters used in this study.

Microfluidic devices were primed with water followed by media using a specialized pressurization system. Approximately 10–20 cells were loaded into the imaging field of the device. Once loaded, the device was set to perfuse only loading media through the growth chamber until the chip had reached thermal equilibrium at 30±1°C (approx. 30 min). The device flows were then changed so that only repressing media flowed through the chamber. The chip was imaged under these conditions for 10 min to establish a non-fluorescent (non-induced) baseline. Finally, the oscillatory drive was initiated and the chamber was imaged every 5 min for 24–48 hr in red, and cyan fluorescence, and transmitted light.

To ensure consistent glucose concentrations between each trial, aliquots from a large stock of repressing media were used. Quantification of on-chip glucose was performed by measuring the mean pixel intensities of non-cell occupied regions within the growth chamber. Flow through the chamber was estimated to be ∼0.5–1 nL/s and transitions in glucose/red dye concentrations were determined to occur on the order of 10–30 seconds. These data allowed for the assumption that the concentration of chemical species within the neighboring perturbation channel was reliably transmitted to cells within the chamber. For each trial, the mean red fluorescence was used as a measure of the glucose concentration state. These data were then scaled so that the maximum value was assumed to represent 0.25% glucose, which was the amplitude of the drive. Mean red fluorescence was then normalized relative to the range of intensity values and reported as $1 - \langle \text{Norm FL} \rangle$ so that the highest trajectory values would correspond to full galactose induction conditions.

Cells were segmented using the transmitted image sequence and a contrast enhancement algorithm. Cell occupied regions of each image were quantified for mean fluorescence in the cyan channel. Population averaged trajectories of cyan fluorescence were normalized and detrended relative to the running trend average. Data trajectories were truncated before the second cycle and after the maximum measured pixel area due to data processing artifacts and reduced segmentation efficiency, respectively. Amplitudes were calculated as the average vertical shift over all cycles from local maxima to local minima in the cyan fluorescence trajectory. Phase shifts were calculated as the average temporal delay between corresponding extrema in the reported induction (red fluorescence) signal and the detrended fluorescence expression responses, scaled by a factor of $2\pi\omega$ where ω is the perturbation frequency in hr^{-1}.

Microfluidic device fabrication

Microfluidic devices were fabricated by replica molding a clear elastomer, PDMS (polydimethylsiloxane), against SU-8 patterned silicon master molds, using well established techniques[6, 7, 8]. Device fabrication occurred in three phases: photolithography, replica molding, and bonding/finishing. Device designs were drawn using AutoCAD 2005 (Autodesk Inc.) and validated by a linear flow modeling program written in Matlab (The Mathworks). Photomasks were printed at 20,000 DPI onto phototransparancy film (Output City, Bandon OR) and used to pattern SU-8 (Microchem Corp.) onto clean silicon wafers. Silicon wafers were spin cleaned using acetone, isopropanol, and methanol, followed by a deionized water rinse and dehydrated for 5 min at 200°C using a contact hot-plate prior to photolithographic patterning. SU-8 photoresist was spun to appropriate depths and processed according to manufacturer's specifications.

Primary fluidic channels (black and green in Fig. 1a in the main text) were fabricated to a

depth of 10 μm. Grooves for the chaotic mixer were patterned to a total depth of 12 μm with the remaining geometric parameters for the mixing units matching those used by Stroock et al. [9] and scaled accordingly to accommodate the designed channel depth. The chamber was fabricated to a depth of 4 μm to accommodate monolayer imaging of *S. cerevisiae*. Channels for on-chip temperature control (orange, Figure 1a in the main text) were patterned to a depth of at least 200 μm.

Poly-dimethylsiloxane (PDMS, Sylgard 184, 2 part silicone encapsulant, Dow Corning) was mixed 1:10 (catalyst:base), degassed, and cast against the SU-8/silicon master mold, curing at 80°C for 1.5 hrs in a dry gravity oven (Fisher Scientific). Prior to casting the PDMS, chlorotrimethylsilane (Sigma) was vapor deposited for 2 min onto the master molds to aid in cured PDMS monolith release. Following release, the PDMS monolith was rinsed in 100% ethanol followed by deionized water. Fluid access ports for media and cell suspension were punched using 20 ga luer stub adapters (McMaster-Carr) while ports for temperature control channels were punched using 16 ga stub adapters. These ports accommodated 23 ga and 18 ga hypodermic steel tubing (Small Parts Inc), respectively, which were used as connection tips for fluidic lines leading to external fluid reservoirs. To remove debris from the port punching process, port holes were flushed with isopropanol and deionized water, and dried with a high velocity stream of 0.2 μm filtered air. Any remaining debris on pattern surfaces was removed using a double application of office grade Scotch Brand Tape (Type 810, 3M).

One day prior to use, the PDMS chips and 24×40 mm coverslips were cleaned using a solvent rinse (acetone, isopropanol, methanol) and exposed to O_2 plasma for 1 min at 50 W in a Technics PEB-II plasma etcher. Treated surfaces were then brought into intimate contact and allowed to anneal overnight at 80°C to ensure maximum bond strength [10].

All fluids used for microfluidic devices were 0.2 μm filtered and autoclave sterilized (when appropriate) to reduce channel occlusion by random debris and bacterial contamination. Similarly, all reservoirs and connecting lines were thoroughly cleaned by flushing with deionized water and isopropanol and autoclave sterilization prior to use. Devices were wetted using sterile water injected simultaneously at all waste outlet ports under 1–3 psi before attaching media and cell suspension reservoirs.

Waveform generation and characterization

To drive concentration waveforms, our device incorporated a fluidic media switch [11, 12] and a series of four chaotic advection mixing units [9]. The fluidic switch, the primary element of the waveform generator, was operated by laminar interface guidance, a method similar to laminar flow focusing (Fig. S1). For example, to "switch" a flow stream, the laminar interface between input flows is guided across an output channel by carefully adjusting the ratio of flow rates between the inputs.

For our device this was done using finely controlled differences in pressure above the corresponding source reservoirs (inputs 1 and 2). By gradually increasing the pressure above the reservoir for input 1 and decreasing the pressure above input 2, the interface would shift to the right of the output channel. Once the interface passed the full width of the output channel the output state of the switch was 100% input 1. Flow from the 0% input and excess from the 100% input was diverted to an auxiliary waste reservoir via bypass channels that flanked the output channel.

The switch on our device was specifically designed to generate intermediate mixing ratios required for waveform production. To do this our device included flow guide channels in the output stream. This utilized the Coanda effect [13] which causes fluid flow to "stick" to boundary surfaces,

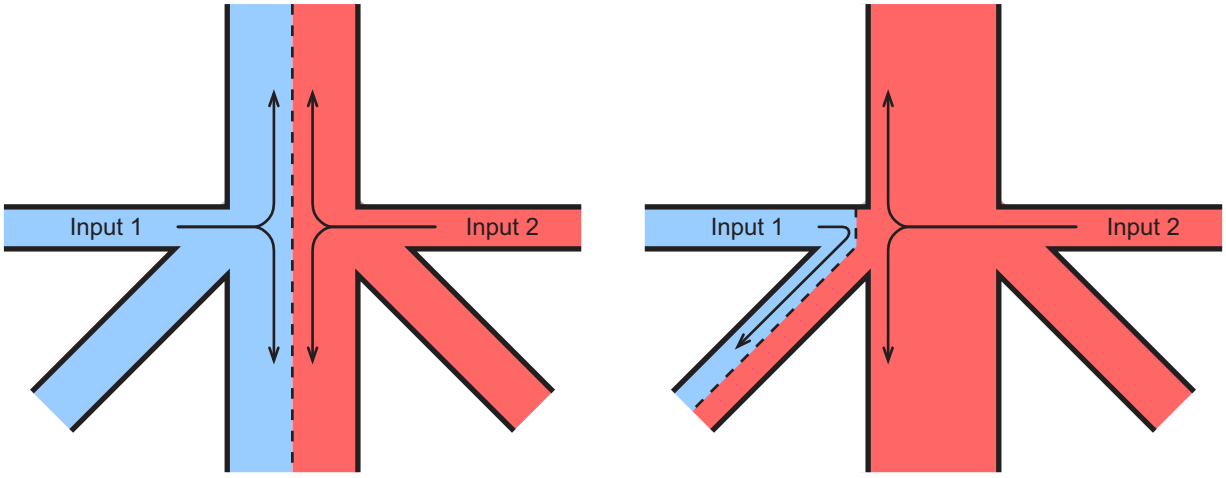

Figure S1: Cartoon schematic of laminar interface guidance.

significantly improving mixing ratio precision and accuracy by allowing the position of the interface to be linearly controlled by the relative pressure difference between the two input reservoirs. Thus, we could produce a continuous linear range of output mixtures from 100% input 1 to 100% input 2 (Fig. S2) over a total pressure difference of 2 inH_2O.

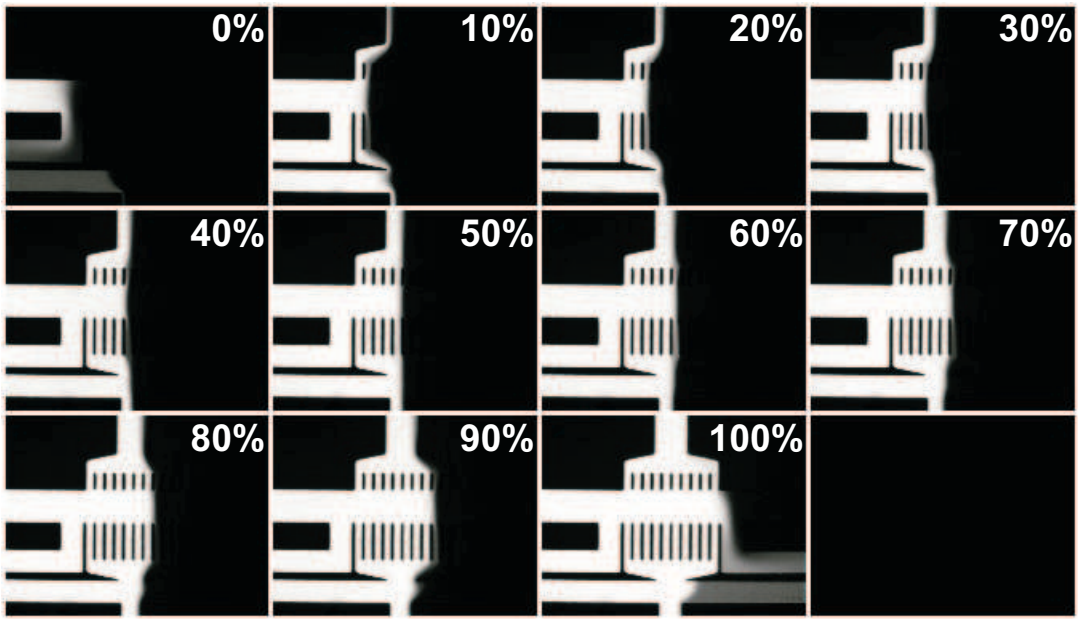

Figure S2: From the upper left to lower right: switch output ratios using a red fluorescent tracer dye from 0% to 100% at 10% intervals.

To automate switch actuation, a pair of card mount servo regulators (Bellofram Inc.) were controlled using LabVIEW (National Instruments) via a two channel analog output board. Output pressures from the regulators were calibrated to a full operating range of 0–12 inH_2O. The run-time operation pressure range was 0–5 inH_2O. All other device flows were driven by gravity based

hydrostatic pressure with all media ports at a base height of 18 inH_2O and waste ports at 10 inH_2O or below.

Operational performance of the waveform generator was evaluated by tracking the distribution of a red fluorescent dye (sulforhodamine 101, Sigma) in $75\times75\mu m^2$ regions in the output channel exiting the switching region and at several points along the mixing train. Measurements within the mixing train were taken at the entrance, middle (after two mixing units), and exit regions. Quantification of the dye distribution was separated into two parameters: concentration and uniformity, measured as regional mean fluorescence and coefficient of variation (C_V), respectively. Ideally uniform regions should exhibit a C_V of zero. Under experimental conditions, this value was approximately 0.05–0.06, due primarily to image noise associated with acquisition. The chaotic mixers smoothed the channel concentration profile from a sharp step function to a uniform distribution across the output channel. This was indicated by an approximate 4-fold drop in region C_V between switch and mixer outlets (Fig. S3a).

The linear range of output mixtures was tested by collecting images from the mixer exit for a rising/falling stair-step routine with 10-second holds at each step for system equilibration. Results of this test (Fig. S3b) show a nearly ideal linear response for a device with flow guide channels (curve B). A device fabricated without these guide channels (curve A) suffered from 20% deviations at the upper and lower extremes of the output range. Fig. S3c shows sinusoidal, triangle, and sawtooth waveforms generated by each device. Output deviations in the device without flow guides were especially noticeable in the triangle and sawtooth waveforms, resulting in a rounding of what should be sharp transitions in measured dye concentration. Under optimized operating conditions, the device was capable of attaining a maximum output frequency of 0.2 Hz. This was determined using a frequency response analysis from 0.05 Hz to 0.4 Hz, which indicated a sharp drop in the output amplitude ratio at the maximal frequency (Fig. S3d).

Transport speed and uniformity within the chamber were tested by pulsing sulforhodamine at 3 mHz and observing the concentration at 12 separate locations within a 40× field (Figs. S3e and S3f). Results of this test show that although deviations exist, they are relatively small, ∼5–10% of the maximum measured value. In addition, the temporal uniformity within the chamber is as desired, with changes in local concentrations at different subregions occurring practically simultaneously. While important for precision control of the microenvironment, the speed of the system also presents a useful means for studying environmental noise effects on gene network dynamics. This could be done by incorporating additional noise components into the output waveforms, or by replicating a purely "noisy" environment by generating a random-step waveform.

Fluorescent Reporter Proteins Used in this Study

We used different fluorescent proteins for different applications. First, a yeast-enhanced CFP (yECFP) was fused to Gal1p in both strains as a readout of network behavior for the original microscopy runs. This was detected on the microscope using a filter set designed for multi-color microscopy. yECFP was used originally in order to maximize spectral separation from the red dye (Sulforhodamine 101) used to monitor the glucose concentration. As a control, we repeated the K699 data with a yEGFP fusion to Gal1p to ensure the absence of artifacts due to the fluorescent fusion, such as time-lags due to the folding rate of the yECFP protein, and also to maximize the signal, since yEGFP is much brighter than yECFP. For the flow cytometry data, we had to create new strains containing Gal1p-yEYFP fusions instead of yECFP, because the laser on the flow cytometer excites at 488nm, which would not excite the yECFP molecule. Finally, for the localization study of Gal2p, we used yEYFP fusions. All of the fusion proteins were constructed using cassettes designed for

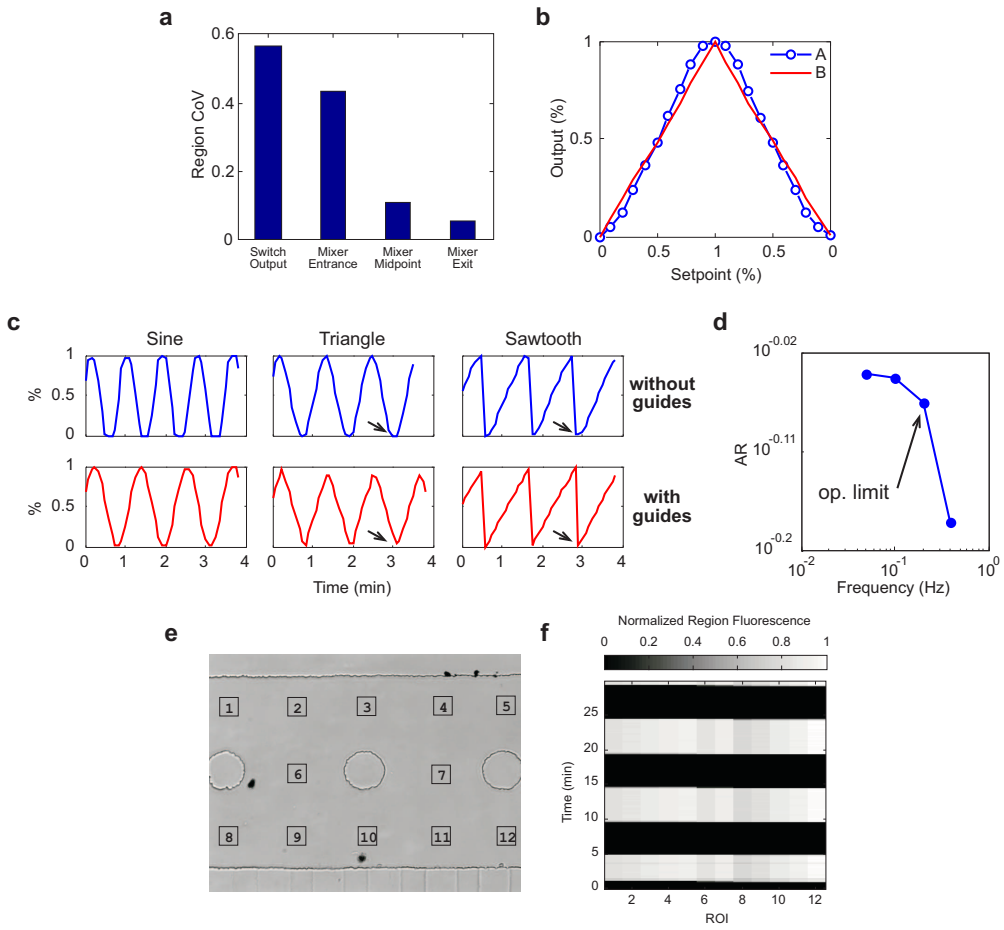

Figure S3: (**a**) Concentration distribution (profile uniformity) at various sections of the device measured as regional coefficient of variation. (**b**) Output response curves for each device. Curve A (—○—) shows the response of a switch without output flow guides. The response has 20% deviations at the extremes of the output range, in contrast to a device with flow guides, curve B (——), which exhibits an ideal linear response. (**c**) Various waveforms generated by the system using devices without (top row) and with (bottom row) flow guides at a nominal frequency of 8.3 mHz. Shown here are sinusoidal, triangle, and sawtooth waves created by the system, measured using a red fluorescent tracer at the exit of the mixer train. Arrows highlight noticeable differences in waveform quality. (**d**) Frequency response analysis of the system showing amplitude ratio for frequencies ranging from 0.05 Hz to 0.4 Hz. The operational threshold is indicated by the sharp drop in the amplitude ratio at 0.2 Hz. (**e**) Map of $15\times15\mu m^2$ regions of interest (ROIs) within a $40\times$ field of view in the growth chamber (black box in Figure 1a) used to measure concentration uniformity. (**f**) Spatio-temporal profile of fluorescent tracer concentration within the growth chamber with environmental changes driven at a nominal frequency of ∼3 mHz. Deviations between regions are relatively small (∼5–10%) and were neglected. Temporal uniformity is ideal.

optimized fluorescent protein tagging in yeast, according to the protocol described in Ref. [1].

Comparison of *GAL2* in *S. cerevisiae* YPH499 and K699

The YPH499 strain of *S. cerevisiae* is derived from the diploid strain YNN216 [14] and is congenic to S288C (ATCC:204508). The S288C yeast strain is known to have a defect in *GAL2*, which encodes the galactose permease. However, many common laboratory strains, such as YPH499,

are S288C derivatives in which *GAL2* has been repaired by homologous recombination. Despite being repaired, the *GAL2* alleles in these strains have been shown to cause significantly impaired galactose uptake [15]. Because this deficiency is poorly understood, we employed both sequencing and localization experiments to shed some light on the poor functionality of *GAL2* in the YPH499 strain.

In order to compare the *GAL2* sequences of the two strains used in this report, genomic DNA was extracted from overnight cultures of YPH499 (MATa, ura3, lys2, ade2, trp1, his3, leu2) (Stratagene) and K699 (MATa ADE2 ura3 his3 trp1 leu2) [16] cells, and the *GAL2* gene, flanked by approximately 400bp on both the 5' and 3' ends was amplified by PCR. Amplification products were purified and blunt ligated into sequencing plasmids, and overlapping sequencing reactions were performed (Eton Bioscience Inc.) to accurately sequence the entire *GAL2* gene. As the K699 strain is considered to contain the wildtype *GAL2* sequence, mutations were documented by looking for errors in the YPH499 sequence with respect to the K699 sequence. Our sequencing results revealed nine point mutations in the YPH499 *GAL2* sequence, yielding the following five amino acid mutations: V8M P50S S90G Y369S R392H.

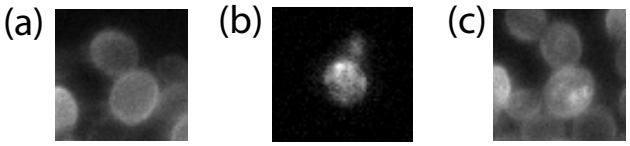

Figure S4: Gal2p activity in K699 and YPH499. **(a)** Gal2p-yEYFP fluorescence in K699 under galactose induction. **(b)** Gal2p-yEYFP fluorescence in YPH499 under galactose induction. **(c)** Gal2p-yEYFP fluorescence in K699 after the cells have been switched from galactose to glucose.

In an attempt to further understand the *GAL2* deficiency in YPH499, we used a fluorescent fusion to GAL2p to compare the localization of the transporter in two strains. Both strains, K699 and YPH499, were transformed with a DNA fragment obtained by PCR to tag GAL2p with the yeast-enhanced Yellow Fluorescent Protein (yEYFP) [1]. Successful transformants of each strain were grown in 2% galactose to fully induce production of the galactose utilization proteins. Overnight cultures were passed in the morning to an OD_{600} of .1 and allowed to grow for 8 hours to reach log phase growth. 10 μl of cell culture was suspended between cover slips and cells were imaged under the microscope at a magnification of 40x. The results of these experiments are shown in Figure S4. The K699 cells (Figure S4(a)) displayed nearly uniform fluorescence throughout the cell with slight rings of fluorescence along the cell perimeter, which is indicative of good localization of the GAL2p transporter to the membrane. The YPH499 cells, however were more anisotropically fluorescent, indicating that the transporter is not being properly localized to the cell membrane (Figure S4(b)). This anisotropy is similar to that seen in K699 cells that are switched from galactose to glucose (Figure S4(c)). The glucose network inhibits the the transport of galactose by removing Gal2p from the membrane, leading to an anisotropic distribution of Gal2p within the cellular volume. It could be that the Gal2p in YPH499 cells is not properly distributed to the plasma membrane. This would likely cause YPH499 cells to actively transport galactose less efficiently than other strains and therefore YPH499 would require more galactose to fully induce the galactose utilization network.

Computational Model

The computational model used in this study represents the combination of two regulatory modules, describing the dynamics of the galactose and glucose networks and their interactions. Glucose is the preferred carbon source in *S. cerevisiae*, and therefore the protein products of the glucose network act to repress the galactose network in several ways. First, Mig1p, a product of the glucose network, down-regulates *GAL1*, *GAL3* and *GAL4* by binding to regulatory sites upstream of the promoters[17]. Second, the glucose network inhibits the transport of galactose by inducing the ubiquitination and subsequent proteolysis of Gal2p[18]. Lastly, it has been speculated that the glucose network can actively degrade mRNA of the galactose network in order to better repress its activity[19]. We found that this last form of repression, when combined with the other two, was crucial to obtaining amplitude response curves from our model that reflect those measured in our experiments. After experimental confirmation of this form of regulation, we incorporated into our model enzymatic decay dynamics for the *GAL1* and *GAL3* transcripts, in which the products of the glucose network govern the concentration of the enzyme.

The galactose module consists of the following reactions

$$\begin{aligned}
Gal_{ex} &\rightarrow Gal && (1)\\
Gal &\rightarrow \emptyset && (2)\\
Gal + g_3 &\rightleftarrows g_3^* && (3)\\
g_i + g_i &\rightleftarrows g_{id}, \quad i = 4, 80 && (4)\\
g_{80d} + g_{4d} &\rightleftarrows g_{4d}^* && (5)\\
g_3^* + g_{80} &\rightleftarrows g_{80}^* && (6)\\
\emptyset &\rightleftarrows m_i, \quad i = 1, 2, 3, 80 && (7)\\
\emptyset &\rightleftarrows g_i, \quad i = 1, 2, 3, 4, 80. && (8)
\end{aligned}$$

Here, Gal_{ex} and Gal are the external and internal galactose, respectively, g_i is the number of the galactose network protein monomers ($i = 1, 2, 3, 4, 80$), m_i is number of the mRNA ($i = 1, 2, 3, 80$), g_{id} is the number of protein dimers ($i = 4, 80$), g_3^* is the number of Gal3p proteins bound to galactose, g_{4d}^* is the number of Gal4p dimers bound to Gal80p dimers, and g_{80}^* is the number of Gal80p proteins bound to the Gal3p-galactose complex. Reactions (1) and (2) are the transport and metabolism of galactose, Reactions (3)-(6) represent the interactions between the galactose proteins and internalized galactose, and Reactions (7) and (8) are the transcription and translation (respectively) of the galactose genes as well as the degradation of the mRNA and protein monomers.

The glucose module is governed by the following reactions:

$$\begin{aligned}
Glu_{ex} &\rightarrow Glu && (9)\\
Glu &\rightarrow \emptyset && (10)\\
\emptyset &\rightleftarrows m_{glu} && (11)\\
\emptyset &\rightleftarrows p_{glu} && (12)\\
p_{glu} + m_i &\rightarrow p_{glu}, \quad i = 1, 3, && (13)
\end{aligned}$$

where Glu_{ex} and Glu are the external and internal glucose, respectively, p_{glu} is the amount of glucose network protein and m_{glu} is the amount of glucose network mRNA. Reactions (9) and (10) are the transport and metabolism of glucose, respectively, Reactions (11) and (13) are the transcription and translation of glucose genes, respectively, and Reaction (13) is the glucose mediate enzymatic decay of *GAL1* and *GAL3* mRNA.

In general, the reaction rates that govern the dynamics of each of the reactions depend on the amount of reactants and enzymes present in the cell. For instance, the rates of transcription in the galactose network depend on the occupation of upstream regulatory sites by Gal4p (which activates the promoters) and the Gal4p-Gal80p complex (which represses). Also, transport of both galactose and glucose into the cell depends on the presence of the respective transporter (e.g. Gal2p for galactose), whereas their metabolization depends on kinases which initiate the metabolic pathways (e.g. Gal1p for galactose).

The model equations, based on mass-action kinetics of the above reactions are:

$$\dot{g}_1 = \beta_1 m_1 - \delta_1 g_1 \tag{14}$$

$$\dot{g}_2 = \beta_2 m_2 - \delta_1 g_2 \tag{15}$$

$$\dot{g}_3 = \beta_3 m_3 - \delta_1 g_2 - k_3[gal]g_3 + k_{-3}g_3^* \tag{16}$$

$$\dot{g}_4 = \beta_4 R(x_{glu}) - \delta_1 g_4 - 2k_{4d}g_4^2 + 2k_{-4d}g_{4d} \tag{17}$$

$$\dot{g}_{80} = \beta_{80} m_{80} - \delta_1 g_{80} - 2k_{80d}g_{80}^2 + 2k_{-80d}g_{80d} - k_{80}g_3^* g_{80} + k_{-80}g_{80}^* \tag{18}$$

$$\dot{m}_1 = \alpha_1 R(x_{glu}) f(g_{4d}, g_{80d}, 4) - \gamma_1 m_1 - \frac{v_{sd} m_1 x_{glu}}{k_{sd} + m_1} \tag{19}$$

$$\dot{m}_2 = \alpha_2 f(g_{4d}, g_{80d}, 2) - \gamma_2 m_2 \tag{20}$$

$$\dot{m}_3 = \alpha_3 R(x_{glu}) f(g_{4d}, g_{80d}, 1) - \gamma_3 m_3 - \frac{v_{sd} m_3 x_{glu}}{k_{sd} + m_3} \tag{21}$$

$$\dot{m}_{80} = \alpha_{80} f(g_{4d}, g_{80d}, 1) - \gamma_{80} m_{80} \tag{22}$$

$$\dot{g}_{4d} = k_{4d}g_4^2 - k_{-4d}g_{4d} - k_r g_{80d} g_{4d} + k_{-r}g_{4d}^* - \delta_1 g_{4d} \tag{23}$$

$$\dot{g}_{80d} = k_{80d}g_{80}^2 - k_{-80d}g_{80d} - k_r g_{80d} g_{4d} + k_{-r}g_{4d}^* - \delta_1 g_{80d} \tag{24}$$

$$\dot{g}_{4d}^* = k_r g_{80d} g_{4d} - k_{-r}g_{4d}^* - \delta_1 g_{4d}^* \tag{25}$$

$$\dot{g}_3^* = k_3 g_3[gal] - k_{-3}g_3^* - k_{80}g_{80}g_3^* + k_{-80}g_{80}^* - \delta_1 g_3^* \tag{26}$$

$$\dot{g}_{80}^* = k_{80}g_{80}g_3^* - k_{-80}g_{80}^* - \delta_1 g_{80}^* \tag{27}$$

$$[\dot{gal}] = R(x_{glu})T([gal], [gal]_e) - \frac{k_{cat} g_1 [gal]}{k_{mgk} + [gal]} - k_3 g_3 [gal] + k_{-3}g_3^* - \delta_1 [gal] \tag{28}$$

$$\dot{m}_{glu} = \frac{\alpha_{glu} + \epsilon_{glu}\left(\frac{[glu]}{c_{glu}}\right)^b}{1 + \left(\frac{[glu]}{c_{glu}}\right)^b} - \gamma_{glu} m_{glu} \tag{29}$$

$$\dot{x}_{glu} = \sigma_{glu} m_{glu} - \delta_{glu} x_{glu} \tag{30}$$

$$[\dot{glu}] = k_{tr2} x_{glu} \frac{[glu]_e - [glu]}{k_{mtr2} + [glu]_e + [glu] + a_{tr2}[glu]_e[glu]/k_{mtr2}} - \frac{\mu_{glu}[glu]x_{glu}}{\kappa_{glu} + [glu]} - \delta_d [glu], \tag{31}$$

where

$$R(x_{glu}) = \frac{\rho^q}{\rho^q + x_{glu}^q} \tag{32}$$

is the repression function due to products of the glucose network that acts on various processes of the galactose network;

$$T([gal], [gal]_e) = k_{tr} g_2 \frac{[gal]_e - [gal]}{k_{mtr} + [gal]_e + [gal] + a_{tr}[gal]_e[gal]/k_{mtr}} \tag{33}$$

is the transport rate of external galactose into the cell [20]; and

$$F(g_{4d}, g_{80d}, N) = \frac{\sum_{i=0}^{N} \binom{N}{i} (K_q K_p g_{4d} g_{80d})^i \sum_{h=1}^{N-i} \binom{N-i}{h} C_P^{h+i-1} C_Q^{i-1} (K_p g_{4d})^h}{\sum_{i=0}^{N} \binom{N}{i} (K_q K_p g_{4d} g_{80d})^i \sum_{h=0}^{N-i} \binom{N-i}{h} C_P^{h+i-1} C_Q^{i-1} (K_p g_{4d})^h} \tag{34}$$

Table S1: Model variable definitions.

Variable	Description
g_1	Gal1p
g_2	Gal2p
g_3	Gal3p
g_4	Gal4p
g_{80}	Gal80p
m_1	*GAL1* mRNA
m_2	*GAL2* mRNA
m_3	*GAL3* mRNA
m_{80}	*GAL80* mRNA
g_{4d}	Gal4p dimer
g_{80d}	Gal80p dimer
g^*_{4d}	Gal4p dimer - Gal80p dimer complex
g^*_3	Gal3p-galactose complex
g^*_{80}	Gal80p-Gal3p-galactose complex
$[gal]$	Internal galactose
m_{glu}	Glucose network mRNA
x_{glu}	Glucose network proteins
$[glu]$	Internal glucose

is the cooperative fractional saturation function describing the number of upstream activation sites occupied on a promoter, given that N sites exist [20]. The variable definitions for the model are given in Table S1.

The model is comprised of two main components, the galactose module, Equations (14)-(28), and the glucose module, Equations (29)-(31). The galactose module was derived from a previously published model[20] that takes into account transcription and translation of the *GAL1*, *GAL2*, *GAL3*, *GAL4* and *GAL80* genes as well as the interactions among themselves and galactose (such as dimerization, transport and metabolism). In contrast, due to the complexity of the glucose network and the relative lack of parameter values known for it, we modeled the glucose module with a heuristic set of equations describing a basic transport regulatory system. Specifically, protein products of the glucose network (x_{glu}) are responsible for transporting external glucose into the cell and internalized glucose acts to induce transcription in the glucose network, giving rise to a positive feedback loop. The glucose proteins are also responsible for repressing genes in the galactose network (akin to Mig1p activity[17]).

To fit our model parameters, we first calibrated the model to galactose induction and glucose repression curves obtained from flow cytometry. Then, parameter values were further modified to reproduce the correct responses to the sinusoidal perturbation studies. Whenever possible, model parameters for the galactose network were chosen to closely match the published estimates given by de Atauri et al. [20]. Due to the widely varied types of experimental data we used to fit the parameters, and the large number of parameters in comparison to data, computational parameter fitting was not practical. Instead, we were forced to adjust each parameter by hand until a robust model was created that accurately predicted the behavior seen in each experiment. The result is a model that accurately reproduces the experimental data obtained from both flow cytometry and

Table S2: Model parameter definitions and values for the galactose network module.

Parameter	Description	K699 value	YPH499 value	units
β_1	Translation rate of Gal1p	9.92	9.92	min^{-1}
β_2	Translation rate of Gal2p	6.94	6.94	min^{-1}
β_3	Translation rate of Gal3p	18.0	18.0	min^{-1}
β_4	Max Translation rate of Gal4p	0.86	0.86	$(molec./cell)/min$
β_{80}	Translation rate of Gal80p	4.00	4.00	min^{-1}
α_1	Max transcription rate of *GAL1*	1.09	1.09	$(molec./cell)/min$
α_2	Max transcription rate of *GAL2*	1.20	1.20	$(molec./cell)/min$
α_3	Max transcription rate of *GAL3*	36.0	36.0	$(molec./cell)/min$
α_{80}	Max transcription rate of *GAL80*	3.00	3.00	$(molec./cell)/min$
δ_1	Degradation rate of gal. proteins and complexes	0.0033	0.0023	min^{-1}
γ_1	Deg. rate of *GAL1* mRNA	0.036	0.036	min^{-1}
γ_2	Deg. rate of *GAL2* mRNA	0.026	0.026	min^{-1}
γ_3	Deg. rate of *GAL3* mRNA	0.036	0.036	min^{-1}
γ_{80}	Deg. rate of *GAL80* mRNA	0.036	0.036	min^{-1}
k_3	Binding rate of g_3 to $[gal]$	5.0×10^{-8}	5.0×10^{-8}	$(cell/molec.)/min$
k_{-3}	Dissociation rate of g_3^*	890	890	min^{-1}
k_{4d}	Binding rate of g_4 to g_4	0.10	0.10	$(cell/molec.)/min$
k_{-4d}	Dissociation rate of g_{4d}	1.0	1.0	min^{-1}
k_{80d}	Binding rate of g_{80} to g_{80}	0.10	0.10	$(cell/molec.)/min$
k_{-80d}	Dissociation rate of g_{80d}	170	170	min^{-1}
k_{80}	Binding rate of g_3^* to g_{80}	0.10	0.10	$(cell/molec.)/min$
k_{-80}	Dissociation rate of g_{80}^*	0.03	0.03	min^{-1}
k_r	Binding rate of g_{4d} to g_{80d}	0.10	0.10	$(cell/molec.)/min$
k_{-r}	Dissociation rate of g_{4d}^*	1.80	1.80	min^{-1}
k_{cat}	Galactose metabolism rate	3350	3350	min^{-1}
k_{mgk}	Galactose metabolism constant	1.29×10^7	1.29×10^7	$molec./cell$
k_{tr}	Galactose transport rate	4350	2000	min^{-1}
k_{mtr}	Galactose transport constant	2.15×10^8	4.30×10^9	$molec./cell$
a_{tr}	Galactose interactive constant	10.0	7.0	(unitless)
K_p	Equilibrium constant of g_{4d} binding to UAS	0.091	0.091	$cell/molec.$
K_q	Equilibrium constant of g_{80d} binding to g_{4d} $(= k_r/k_{-r})$	0.0556	0.0556	$cell/molec.$
C_P	Cooperative binding constant of g_{4d} to UAS	1	1	(unitless)
C_Q	Cooperative binding constant of g_{80d} to g_{4d}-UAS complexes	30	30	(unitless)
$[gal]_e$	External galactose concentration	2.366×10^8	2.366×10^8	$molec./cell$

Table S3: Model parameter definitions and values for the glucose network module.

Parameter	Description	K699 value	YPH499 value	units
α_{glu}	Basal transcription rate of glucose DNA	215	215	$(molec./cell)/min$
ϵ_{glu}	Activated transcription rate of glucose DNA	6.452×10^5	6.452×10^5	$(molec./cell)/min$
σ_{glu}	Translation rate of glucose proteins	0.4	0.4	min^{-1}
δ_{glu}	Degradation rate of glucose proteins	0.1	0.1	min^{-1}
γ_{glu}	Degradation rate of glucose mRNA	0.0633	0.0629	min^{-1}
δ_d	Dilution rate of glucose	0.0033	0.0023	min^{-1}
c_{glu}	Hill constant for glucose induction	1.075×10^7	1.075×10^7	$molec./cell$
b	Hill coefficient for glucose induction	1.8	1.8	(unitless)
k_{tr2}	Glucose transport rate	4350	4350	min^{-1}
k_{mtr}	Glucose transport constant	6.022×10^8	6.022×10^8	$molec./cell$
a_{tr}	Galactose interactive constant	1.0	1.0	(unitless)
μ_{glu}	Glucose metabolism rate	5350	5350	min^{-1}
κ_{glu}	Glucose metabolism constant	1.29×10^7	1.29×10^7	$molec./cell$
$[glu]_e$	External glucose concentration	0-2.957×10^8	0-2.957×10^8	$molec./cell$
ρ	Hill constant for gal. repression	1.29×10^7	1.29×10^7	$molec./cell$
q	Hill coefficient for gal. repression	0.8	0.8	(unitless)
v_{sd}	Glucose induced mRNA degradation rate	9.30×10^{-6}	2.325×10^{-6}	min^{-1}
k_{sd}	Glucose induced mRNA degradation constant	30	30	$molec./cell$

sinusoidal perturbation experiments. Parameter definitions and values used in both versions of the model (K699 and YPH499) are given in Tables S2 and S3.

To take into account fluctuations in the glucose signal due to experimental errors, we decided to use fluorescence data taken directly from each experiment as inputs into our model. The reservoir containing the glucose also contained a red fluorescent dye, allowing us to take red fluorescent images. The amount of red fluorescence was then proportional to the concentration of glucose in the chamber at any given time (see details in Methods). After scaling the fluorescence data, time series were created that could be fed into the numerical model as the time-dependent parameter $[glu]_e$.

Decay rates of *GAL1* and *GAL3* mRNA: experimental procedures and comparison to model predictions

To measure the degradation rates of *GAL1* and *GAL3* transcripts, we first cloned *GAL1* and *GAL3*, including 5' and 3' UTR sequences, from genomic DNA by PCR with the following primer pairs: *GAL1* (5' GGATCCTATGAAGAGGAAAAATTGGCAGTAACCTGGCCCC 3' and 5' GCGG CCGCAGGTATCCAAAACGCAGCGG 3'); *GAL3* (5' GGATCCCTATATGTTGATAATTAG CGTTGCCTCATCAATGCG 3' and 5' GCGGCCGCGAAGACGATGGATGCACTGAGAATG TAATGCACT 3'). Doxycycline-repressible expression plasmids were made by subcloning *GAL1* (pBB14) and *GAL3* (pBB15) into a vector for Tet activator (tTA) driven expression, pCM185 (Euroscarf). To create strains with tTA-driven *GAL1* and *GAL3*, the endogenous genes were first deleted from K699 by integration of *KanMX6* knock-out cassettes. Each knock-out strain was then transformed with pBB14 or pBB15.

To measure the half-life of *GAL* transcripts in galactose, single colonies were grown to saturation in selective medium containing 2% raffinose, then diluted into YEP +2% galactose and continued growing for 4–6 hr until OD_{600} 0.3. In experiments where *GAL* gene expression was being driven by tTA, 2 μg/ml doxycycline was added to the gal-induced culture at $t = 0$ min. Samples (1 mL) were taken at indicated times after doxycycline addition, pelleted, and frozen in liquid nitrogen. To measure the RNA half-life of *GAL* transcripts in glucose, the starting raffinose cultures were diluted into YEP + 2% glucose and grown 4–6 hr to an OD_{600} 0.3. Time course samples were collected as described for the gal-induced cultures.

Total RNA was prepared from frozen time course samples using the RNeasy miniprep kit (QIAGEN), according to the manufacturer's protocol. To synthesize cDNA, 1 μg total RNA was used as template in a 20 μl reverse transcriptase reaction with oligo-dT and omniscript RT (QIAGEN), according to the manufacturer's instructions. Forty cycles of qPCR were performed using QuantiTech SYBR green PCR mix (QIAGEN) and iCycler iQ real-time PCR detection system (BioRad). The gene-specific primers were as follows: *ACT1* (5' CAGAGCCCCAGAAGCTTTGTTCCATC C 3' and 5' CTGGAGGAGCAATGATCTTGACCTTCATGG 3'); *GAL1* (5' GGGCTTTAGTG TTGACGATGTCGCAC 3' and 5' CAACCACCCCAGCCAGCTCCG 3'); *GAL3* (5' GTACATG AAGCCTCTACGGCGC 3' and 5' GAGACGGGAGCCGAAAGAACCA 3').

For each qPCR sample, the raw score, given as the cycle number at which the amount of PCR product reached a threshold level, was first subtracted from 40 to reflect the number of cycles remaining in the experiment. The data for *GAL1* or *GAL3* were then normalized to the *ACT1* data. The relative concentrations of *GAL1* and *GAL3* transcripts can then be derived from the normalized qPCR data with the formula, $[mRNA] \propto \exp(\ln 2 * m)$, where m is the number of cycles remaining in the experiment. To obtain the half-lives of the transcripts, the time points for each transcript were fit with a least squares routine to the line $m(t) = m_0 - t/t_{1/2}$, where m_0 is the

Table S4: Half-life measurements for *GAL1* and *GAL3* mRNA.

Sugar	Promoter	$t_{1/2}$ of *GAL1* mRNA	$t_{1/2}$ of *GAL3* mRNA
Galactose	$P_{O_{tet7}}$	17 min	16 min
Glucose	$P_{GAL1/3}$ in K699	3 min	2 min
	$P_{GAL1/3}$ in K699-1cc2yv (GAL1-yECFP)	4 min	3 min
	$P_{O_{tet7}}$	4 min	9 min

estimated relative concentration at time $t = 0$ and $t_{1/2}$ is the half-life.

In order to test the prediction that *GAL1* and *GAL3* mRNA half-lives are sensitive to glucose, we first measured the half-lives of these transcripts in galactose-induced cells after glucose addition. Consistent with our model's prediction, we found that in two different strains *GAL1* and *GAL3* mRNAs decayed rapidly ($t_{1/2} \approx 3$ min) after glucose addition. Table S4 shows the experimentally measured half-lives for both transcripts. To measure the half-lives of these transcripts in cells growing only in galactose, we constructed strains that express *GAL1* and *GAL3* from an inducible promoter that is not affected by the carbon source. We chose to use the tTA activator in combination with the O_{tet7} promoter because the levels of gene expression from this system have been reported to approximate expression from the *GAL1* promoter [21]. In this system, gene expression is rapidly repressed by addition of small amounts of doxycycline to the growth medium. We cloned the full length *GAL1* and *GAL3* genes, including their potentially regulatory 5' and 3' UTRs, into tTA expression plasmids. We found that when cells were grown in galactose, the half-lives of both *GAL1* and *GAL3* transcripts after doxycycline addition were approximately 17 min, significantly longer than what we measured for the endogenous genes after glucose repression. To confirm that the doxycycline was effectively repressing the expression of the tTA driven genes, we measured the half-life of *GAL1* mRNA in glucose cultures after doxycycline addition and found it to be 4 min. These results strongly support the model that the decay rates of gene transcripts in the galactose network are sensitive to glucose. The mechanism of this response to glucose is not currently known. In general, the untranslated regions of mRNA transcripts are responsible for turnover rates. We found the decay rate of the *GAL1-yECFP* transcript in glucose to be similar to that of untagged *GAL1*, suggesting that the 3' UTR is not mediating the glucose sensitivity of *GAL1*. Therefore, consistent with what has been reported for other glucose sensitive mRNAs, we suspect that it is the 5' UTRs of *GAL1* and *GAL3* transcripts that promote degradation in the presence of glucose. Unlike the case for *GAL1*, the half-life of the tTA-driven *GAL3* transcript in glucose was longer (although still shorter than in galactose) than that of the endogenous *GAL3* mRNA. One possibility is that the length of the 5' UTR on the plasmid born *GAL3* mRNA is different from that of *GAL3* transcripts from the native promoter, which could be affecting the structure of the glucose-responsive element.

Because the form of glucose mediated decay in the model is enzymatic, true half-life predictions are problematic (since enzymatic decay does not lead to half-lives, *per se*). However, we are able put an upper bound on the half-lives by assuming that the enzymatic decay term is in the exponential regime (i.e. the amount of mRNA is much less than the constant k_{sd}). In this case, the glucose mediated decay rate will be proportional to $v_{sd} \cdot x_{glu}/k_{sd}$. By integrating the full model, we obtain a time series for the variable x_{glu}, and from that time series we can calculate the maximum possible decay rate as $v_{sd} \cdot \max[x_{glu}(t)]/k_{sd}$. From these estimates, half-lives can be predicted. Depending

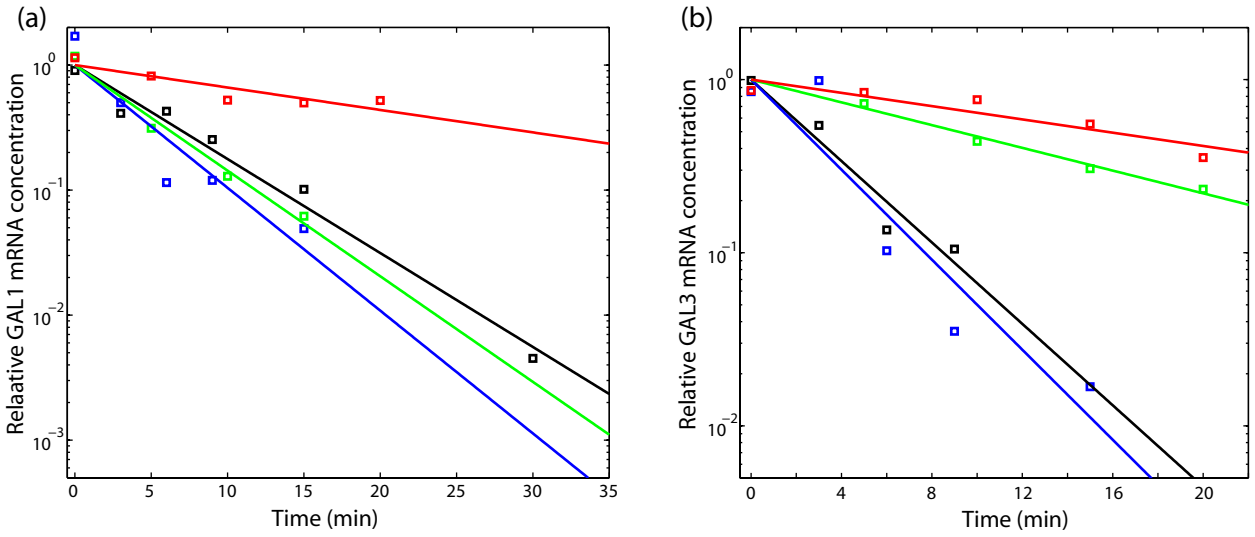

Figure S5: Decay curves obtained from qPCR. Squares indicate experimental data, while solid lines are best-fit lines obtained from least-squares curve fitting. Colors represent different conditions and constructs; *Red*: $P_{O_{tet7}}$ driven genes in galactose; *Green*: $P_{O_{tet7}}$ driven genes in glucose; *Blue*: Endogenous genes of the K699 strain in glucose; *Black*: Endogenous genes of the K699-1cc2yv (GAL1-yECFP) strain in glucose. **(a)** Decay of *GAL1* mRNA. *(b)* Decay of *GAL3* mRNA. Values for the experimentally measured half-lives are given in Table S4.

on the frequency of the drive, these estimates put a lower bound on the half-lives from about 2-4 min, which is very close to the experimentally measured values.

Induction and Repression Experiments

The induction and repression curves were obtained using flow cytometry to measure the fluorescence values of 10^5 individual cells in each media condition. Both strains, K699 and YPH499, were transformed with a DNA fragment obtained by PCR to tag GAL1p with the yeast-enhanced Yellow Fluorescent Protein (yEYFP) [1]. For the induction curves, cells were grown for 24 hours in selective medium containing 2% (w/v) raffinose as the carbon source, and cultures were passed as necessary to maintain log phase growth. After 24 hours, cells were diluted into medium containing 2% raffinose plus a certain amount of galactose, ranging from 0.0001% to 2.2%. After six generations, cells were assayed at mid-log phase at an absorbance (OD_{600}) of $.5 \pm .05$. Expression data were collected using a Becton-Dickinson FACSCalibur flow cytometer with a 488 nm argon excitation laser and a 515 nm to 545 nm emission filter. Forward scatter and fluorescence values were collected for 10^5 cells, and MATLAB (The MathWorks, Inc.) was used to process the data to obtain the mode of each fluorescence distribution. Repression curves were obtained using a similar protocol. Cells were grown for 24 hours in selective medium containing 2% raffinose plus .2% galactose, mimicking the background inducing medium used in the microscope runs. Cells were then passed into medium containing 2% raffinose and 0.2% galactose plus a certain amount of glucose, ranging from 0.0001% to 2.2%. After six generations, the cells were assayed as described above. Figure S6 shows the results of these experiments and the fits of the numerical models for both strains.

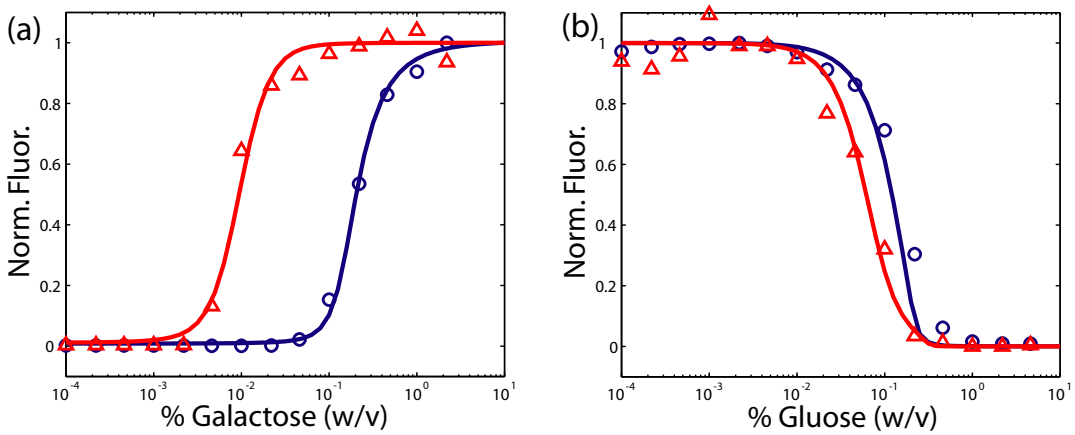

Figure S6: Induction and repression curves for the two strains. **(a)** Galactose induction curves. Shown are the experimentally obtained data (symbols) and numerical fit from the model (solid lines) for the K699 (red) and YPH499 (blue) strains. **(b)** Glucose repression curves. Shown are the experimentally obtained data (symbols) and numerical fit from the model (solid lines) for the K699 (red) and YPH499 (blue) strains.

References

[1] Mark A Sheff and Kurt S Thorn. Optimized cassettes for fluorescent protein tagging in Saccharomyces cerevisiae. *Yeast*, 21(8):661–670, Jun 2004.

[2] David Ross, Michael Gaitan, and Laurie E Locascio. Temperature measurement in microfluidic systems using a temperature-dependent fluorescent dye. *Anal. Chem.*, 73(17):4117 – 4123, 2001.

[3] S. K. W. Dertinger, D. T. Chiu, N. L. Jeon, and G. M. Whitesides. Generation of gradients having complex shapes using microfluidic networks. *Anal. Chem.*, 73(6):1240–6, Mar 2001.

[4] N. L. Jeon, S. K. W. Dertinger, D. T. Chiu, I. S. Choi, A. D. Stroock, and G. M. Whitesides. Generation of solution and surface gradients using microfluidic systems. *Langmuir*, 16(22):8311–6, 2000.

[5] A. D. Stroock, S. K. Dertinger, G. M. Whitesides, and A. Ajdari. Patterning flows using grooved surfaces. *Analytical Chemistry*, 74(20):5306–5312, 2002.

[6] G. M. Whitesides, E. Ostuni, S. Takayama, X. Y. Jiang, and D. E. Ingber. Soft lithography in biology and biochemistry. *Ann. Rev. Biomed. Eng.*, 3:335–373, 2001.

[7] G. M. Whitesides, J. Jiang, S. Sia, V. Linder, B. Parviz, A. Sigel, and J. Lee. Soft lithography and bioanalysis. *Abstr. Paper Am. Chem. Soc.*, 227:U113–U113, 2004.

[8] Y. N. Xia and G. M. Whitesides. Soft lithography. *Angew. Chem. Int. Edit.*, 37(5):550–75, Mar 1998.

[9] Abraham D. Stroock, Stephan K. W. Dertinger, Armand Ajdari, Igor Mezic, Howard A. Stone, and George M. Whitesides. Chaotic mixer for microchannels. *Science*, 295(5555):647–651, 2002.

[10] Z. Y. Wu, N. Xanthopoulos, F. Reymond, J. S. Rossier, and H. H. Girault. Polymer microchips bonded by O_2-plasma activation. *Electrophoresis*, 23(5):782–90, Mar 2002.

[11] A. Groisman, C. Lobo, H. Cho, J. K. Campbell, Y. S. Dufour, A. M. Stevens, and A. Levchenko. A microfluidic chemostat for experiments with bacterial and yeast cells. *Nature Methods*, 2:685–689, 2005.

[12] G. B. Lee, B. H. Hwei, and G. R. Huang. Micromachined pre-focused m x n flow switches for continuous multi-sample injection. *Journal of Micromechanics and Microengineering*, 11(6):654–661, 2001.

[13] C. C. Hong, J. W. Choi, and C. H. Ahn. A novel in-plane passive microfluidic mixer with modified tesla structures. *Lab on a Chip*, 4(2):109–113, 2004.

[14] R. S. Sikorski and P. Hieter. A system of shuttle vectors and yeast host strains designed for efficient manipulation of DNA in Saccharomyces cerevisiae. *Genetics*, 122(1):19–27, May 1989.

[15] J. R. Rohde, J. Trinh, and I. Sadowski. Multiple signals regulate gal transcription in yeast. *Mol. Cell Biol.*, 20(11):38803886, 2000.

[16] J. M. Raser and E. K. O'Shea. Control of stochasticity in eukaryotic gene expression. *Science*, 304(5678):1811–4, Jun 2004.

[17] M. Verma, O. J. Bhat, and K. V. Venkatesh. Steady-state analysis of glucose repression reveals hierarchical expression of proteins under Mig1p control in *Saccharomyces cerevisiae*. *Biochem. J.*, 388:843–849, 2005.

[18] J. Horak and D. H. Wolf. Glucose-induced monoubiquitination of the Saccharomyces cerevisiae galactose transporter is sufficient to signal its internalization. *J. Bacteriol.*, 183(10):3083–3088, May 2001.

[19] M. Ronen and D. Botstein. Transcriptional response of steady-state yeast cultures to transient perturbations in carbon source. *Proc. Natl. Acad. Sci. USA*, 103:389–394, 2006.

[20] P. de Atauri, D. Orrell, S. Ramsey, and H. Bolouri. Evolution of 'design' principles in biochemical networks. *Syst. Biol.*, 1(1):28–40, 2004.

[21] E. Garí, L. Piedrafita, M. Aldea, and E. Herrero. A set of vectors with a tetracycline-regulatable promoter system for modulated gene expression in *Saccharomyces cerevisiae*. *Yeast*, 13:837–848, 1997.